Mitigation of Coupled Wind-Wave-Earthquake Responses of a 10 MW Fixed-Bottom Offshore Wind Turbine

Yang YANG [a,b,*], Musa BASHIR [b], Chun LI [a], Constantine MICHAILIDES [c],Jin WANG [b]

[a.] School of Energy and Power Engineering, University of Shanghai for Science and Technology, Shanghai, 200093, P.R. China

[b.] Department of Maritime and Mechanical Engineering, Liverpool John Moores University, Byrom Street, L3 3AF, Liverpool, UK

[c]. Department of Civil Engineering and Geometrics, Cyprus University of Technology, Saripolou 2-8, 3036, Limassol, Cyprus

Abstract: In this paper we present a study on the mitigation of dynamic responses of a 10 MW monopile offshore wind turbine under coupled wind-wave-earthquake excitations. We have developed and validated the generic seismic coupled analysis and structural control architecture tool to overcome the limitation of numerical tools when examining the wind-wave-earthquake coupling effects. We investigated the dynamic responses of a 10 MW monopile offshore wind turbine under different loading combinations and found that the earthquake loading increases the tower-top displacement and pile-cap moment by 47.6% and 95.1%, respectively, compared to the wind-wave-only condition. It is found that the earthquake-induced vibration in the fore-aft direction is mitigated by the wind and wave loadings due to the energy dissipated by the aerodynamic and hydrodynamic damping. In addition, the tower responses are dominated by the earthquake excitation. In order to alleviate the tower vibration induced by the earthquake, we implemented the structural control capability within the tool using tuned mass dampers. The tuned mass dampers with appropriately selected design parameters achieve a larger mitigation on the tower-top

displacement for the earthquake-only condition compared to the coupled-loading scenario. The reason is that the tuned mass damper is only effective in mitigating tower vibration, and it is not capable of reducing the tower elastic deformation which is the major contribution of the tower displacement for the coupled-loading condition. In addition, we have found that a heavier tuned mass damper requires a lower tuned frequency to achieve a larger mitigation. A configuration for the mitigation control of the 10 MW offshore wind turbine is suggested by using a 5% mass ratio of the tuned mass damper.

Keywords: Offshore Wind Turbines; Tuned Mass Dampers; Wind-Wave-Earthquake Analysis; Structural Control; Earthquake Excitation;

1 Introduction

The climate action demands lower emissions of greenhouse gases by decreasing energy consumption and transitioning to low-carbon or zero-carbon resources. Development of renewable energy resources offers the most efficient action in reducing carbon emissions for moderating the global warming [1]. According to the study by Liang et al. [2], the average CO2 abatement cost decreases by 0.7 EUR for every 1% increase of the capacity factor of renewable power resources. Moreover, the renewable energy sector has been at the forefront of realizing the sustainability goals by playing a significant role in providing access to basic and clean electric power to people, especially those living in developing countries and remote areas with huge difficulties in accessing electricity grid facilities. In addition, the renewable energy sector has continued to serve as a vehicle for social mobility in providing 10.3 million jobs worldwide as estimated by the International Renewable Energy Agency (IRENA) [3].

Further development of renewable energy technologies will produce significant economic and environmental benefits in moving humanity towards achieving sustainability goals.

Offshore wind offers a promising pathway to accelerating transitions to sustainability goals due to its availability and high capacity factor. As indicated in the outlook report of the International Energy Agency (IEA) [4], the offshore wind energy market has expanded by nearly 30% per year between 2010 and 2018, and the global offshore wind capacity is expected to increase by over 20 GW per year in the coming decade. It is noted that there are more than 40% of Offshore Wind Turbines (OWTs) expecting to be installed in the coastal areas of China, Mediterranean and the United States, which are earthquake-prone. The seismic hazards necessitate the examination of the coupling effects between wind, wave and earthquake loadings in the design of OWTs operating in these areas.

Early-stage seismic studies employed the response spectrum method [5-6] to estimate the load demand of a wind turbine under an earthquake event. The linear modal properties including the mode shapes and mass distribution were used as recommended in the seismic design codes of conventional buildings [7]. However, the difference between a wind turbine and conventional buildings is that the aerodynamic load acting on the rotor is as significant as earthquake excitations. In order to consider the wind effect, these studies [8-11] simplified the aerodynamic loads as time-varying rotor thrusts that were calculated externally in an uncoupled manner, meaning that the pitch velocity of the rotor induced by the tower vibration under an earthquake event was neglected. The aerodynamic load, however, is sensitive to the relative speed between inflow wind and rotor, especially for large-scale OWTs. The coupled effect of wind and earthquake loadings must be examined in the seismic analysis of wind

68 turbines.

69 In order to address the research need, a seismic module was added into the commercial
70 software tool, Bladed [12]. A recent study by Santangelo *et al.* [13] investigated the influence
71 of the coupling effect between wind and earthquake for a 5 MW wind turbine using Bladed.
72 Similarly, Asareh [14-15] implemented the seismic analysis capability into FAST by
73 developing an additional module that used the big-mass method to calculate earthquake
74 excitations [16-17]. A fictive platform with big-mass rigidly connecting the wind turbine base
75 was placed beneath the ground. The stiffness and damping of the platform, depending on the
76 mass, were used to determine the earthquake loads. Asareh *et al.* [18] investigated the
77 dynamic behaviours of a 5 MW wind turbine influenced by earthquake intensity and wind
78 speed using the FAST-Seismic. However, it is noted that the definition of the fictive mass
79 depends on the experience of users. Furthermore, this method is incapable of considering the
80 soil-structure interaction (SSI) effect that would be more significant under an earthquake
81 event. Yang *et al.* [19] further improved the method of earthquake load calculation used in
82 FAST-Seismic by using the Wolf model. The influence of aerodynamic damping on the
83 seismic behaviour of a 5 MW wind turbine was investigated for different earthquake loading
84 scenarios.

85 The studies reviewed above investigated the seismic behaviour of land-based wind
86 turbines. As numerous offshore wind farms are located in earthquake-prone sites such as
87 south-eastern coastal areas of China, coastal areas of south-eastern Europe and the west
88 coastal areas of the US, it is vital to perform seismic analysis of OWTs. Kim *et al.* [20]
89 conducted a fragility analysis of a 5 MW monopile OWT subjected to earthquake loadings

under the parked state. The SSI was modelled using *p-y* curves. Mo *et al*. [21] developed a weak-coupled model of a 5 MW OWT in OpenSees. The fragility of the support structure was investigated under different operating conditions. Alati *et al.* [22] compared the dynamic responses of two types of fixed-bottom OWTs subjected to wind and earthquake loadings using Bladed. The SSI effect was examined using the linear coupled-springs model. Yang *et al.* [23-24] investigated the linear and nonlinear SSI effects on the seismic behaviour of a 5 MW OWT using a newly developed numerical tool based on FAST. The dominance of wind, wave and earthquake loadings was discussed for the 5 MW wind turbine.

However, in all the above mentioned literatures the focus has been on wind turbines whose capacity is up to 5 MW. Due to the demand for reducing installation and maintenance costs of OWTs as part of requirements for reducing Levelised Cost of Electricity (LCoE), the development of 10 MW-class wind turbines is attracting significant attention. Consequently, it is imperative to investigate the coupling effects of wind, wave and earthquake loadings for 10 MW OWTs located within earthquake-prone areas including some particular coastal areas of Europe, China and the US. Furthermore, mitigation studies are required to reduce the risk of potential damage caused by an earthquake.

In order to address the identified research gap, this study aims to investigate the dynamic behaviour of a 10 MW OWT subjected to coupled wind wave and earthquake loadings. In addition, a study on mitigation of the coupled dynamic responses is examined to reduce the risk of potential damage during an earthquake event. In order to conduct the research and achieve its aims, a generic Seismic Coupled Analysis and Structural Control Architecture (SCASCA) is developed to conduct fully coupled simulations of OWTs subjected to wind,

112 wave and earthquake loadings. The seismic analysis capability is implemented into an open
113 source numerical tool, FAST (version 7.02) [25], by modifying its source code with regards to
114 the structural modelling. In addition, the SCASCA tool is further improved to be capable of
115 performing structural control analysis based on the Tuned Mass Damper (TMD) [26] for
116 mitigating the coupled responses. The SCASCA offers a generic capability of performing
117 seismic analysis of different wind turbines compared to FAST-Seismic developed by Asareh
118 *et al.* [14], since the approach of earthquake load calculation employed in SCASCA is
119 independent of the researcher's experience. The superiority of SCASCA compared to Bladed
120 is that SCASCA is capable of examining the vertical excitation of an earthquake. In addition,
121 the frequency contents of the input ground motion can be adjusted in order to be consistent
122 with the target response spectrum of a specific site.

123 Fig. 1 presents the research tasks and objectives of this paper. With the use of SCASCA,
124 dynamic responses of the 10 MW monopile OWT [27] under different loading combinations
125 are obtained and compared in order to illustrate the dominance of the environmental loadings.
126 The effectiveness of a TMD in alleviating tower vibration caused by the coupled loads is
127 investigated. Rational parameters of a TMD with a specified mass ratio are obtained by
128 conducting parametric and sensitivity analyses of the control parameters. The maximum
129 tower-top displacement is reduced significantly by an appropriate TMD under both coupled
130 and earthquake-only environmental conditions.

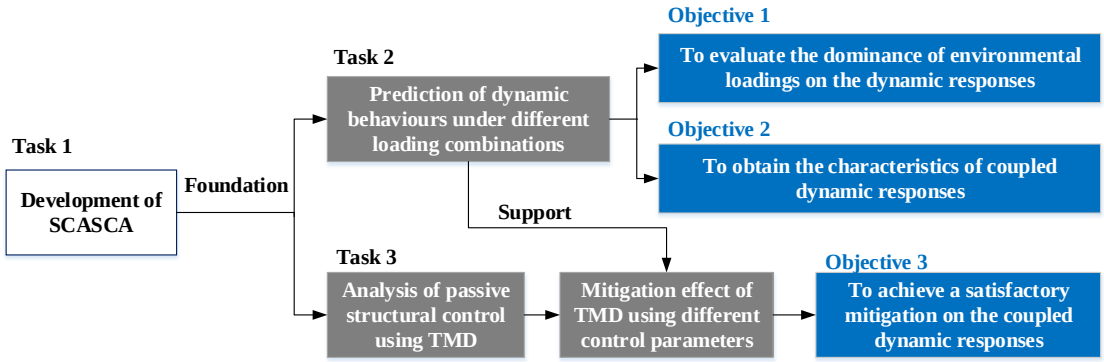

Fig. 1: Research tasks and objectives of this paper

2 Development of SCASCA

A generic tool named SCASCA is developed in order to investigate and moderate the seismic behaviour of a 10 MW OWT under coupled wind-wave-earthquake loadings. The capabilities of seismic analysis and structural control are implemented within the FAST (version 7.02) numerical tool [25]. The subsequent sections present an overview of the original FAST as well as of the development of SCASCA.

2.1 Overview of FAST

National Renewable Energy Laboratory (NREL) developed a fully coupled aero-hydro-servo-elastic tool, FAST, for the design of horizontal axis wind turbines [25]. The original version of FASTv7.02 used in this study integrates four major modules: AeroDyn, ElastDyn, ServoDyn and HydroDyn. Aerodynamic and hydrodynamic loads are computed in the AeroDyn and HydroDyn modules, respectively. The ServoDyn module deals with the adjustments of blade pitch angles and generator speed for normal power production through a dynamic link library. In the ElastDyn module, the wind turbine is modelled as a multi-body dynamic system consisting of rigid and flexible structural elements. The equation of motion of the dynamic system is derived using the Kane method [28]. The linear modal approach is

149 used to predict aero-elastic responses of the blades and tower. The capabilities of seismic
150 analysis and structural control can be implemented by modifying the source code of the
151 ElastDyn module.

152 FAST has been extensively used in industrial and academic studies due to its
153 well-validated accuracy and credibility. The open source nature of FAST encourages
154 researchers to implement new capabilities for the design of wind turbines. FAST is an ideal
155 option to be used as the foundation for the development of SCASCA.

156 *2.2 Implementation of seismic analysis capability*

157 The big-mass method is one of the commonly-used approaches in the calculation of
158 seismic loads of civil engineering structures. It assumes that the structure above the ground
159 behaves as a rigid body under the influence of a fictive big-mass body beneath the ground.
160 The fictive big-mass body follows the input ground motion, resulting in seismic load acting
161 on the structure. This method is efficient in capturing intense variations of structural responses
162 during an earthquake event. The implementation of this method only requires an estimation of
163 the seismic load based on simple equations and without the need to modify the equation of
164 motion of the wind turbine. Asareh *et al*. [14] used this method to develop the Seismic module
165 and integrated it into FAST. However, it is noted that the definition of the fictive mass
166 depends on the experience of the users. Furthermore, this method is incapable of considering
167 the SSI effect that would be more significant under an earthquake event.

168 In order to address the limitations of the big-mass method, this study modifies the
169 equation of motion of the wind turbine in FAST based on a generic theory that has been
170 extensively applied in civil engineering. For a monopile OWT, FAST treats the pile and tower

as one integrated support structure. FAST employs the linear modal approach in the structural modelling of the support structure. The equation of motion for each of the considered i^{th} modal degrees of freedom (DOFs) of the support structure subjected to wind, wave and earthquake loadings is derived as follows:

$$\omega_i^2 q_i + 2\xi_i \omega_i \dot{q}_i + \ddot{q}_i = (a_{\mathrm{eq}} \gamma_i + F_{aero,i} + F_{hydro,i} + F_{gra,i}) / m_i \quad (1)$$

where q_i, $\dot{q}_i$ and $\ddot{q}_i$ are, respectively, the modal displacement, velocity and acceleration of the i^{th} mode. ω_i and ξ_i are the angular frequency and damping ratio of the i^{th} mode, respectively. a_{eq} is the input earthquake acceleration. $F_{aero,i}$, $F_{hydro,i}$ and $F_{gra,i}$ are, respectively, the generalized aerodynamic, hydrodynamic and gravity loads corresponding to the i^{th} mode. m_i is the modal mass associated with the i^{th} mode. γ_i is the earthquake participation factor associated with the i^{th} mode that is denoted as:

$$\gamma_i = \int_0^H \rho(h) \cdot \phi_i(h) \cdot \mathrm{d}h \quad (2)$$

where H is the length of the support structure. $\rho(h)$ is the mass density of the support structure and $\phi_i(h)$ is the normalized modal shape of the i^{th} mode of the support structure.

The rotor-nacelle-assembly (RNA) is simply treated as a lumped mass atop the support structure for the seismic load calculation. The corresponding seismic load of the RNA, $F_{\mathrm{eq,RNA}}$, is derived as:

$$F_{\mathrm{eq,RNA}} = a_{\mathrm{eq}} \cdot m_{\mathrm{RNA}} \quad (3)$$

where m_{RNA} is the total mass of RNA.

It is apparent that the prediction of seismic load only depends on the modal shapes of the structure and the input earthquake acceleration. The method implemented in this study is generic and applicable to an arbitrary wind turbine. Furthermore, the SSI effect is considered

193 properly using the Winkler spring-dashpot model when calculating the modal shapes of the
194 structures.

195 The seismic loads are added into the generalized forces within FAST when modelling the
196 equation of motion of the wind turbine. The source code of FAST is modified accordingly
197 based on the equations presented above in order to implement the fully coupled seismic
198 analysis capability.

199

200 *2.3 Structural control*

201 In order to moderate and mitigate the dynamic responses of an OWT subjected to
202 earthquake loadings, a passive structural control module is developed using the TMD method.
203 The basic concept of the TMD method is to place a mass damper at an appropriate location
204 for dissipation of energy from external excitations. In this study, two independent TMDs are
205 orthogonally placed at the tower-top to mitigate longitudinal and lateral responses of the
206 support structure due to coupled wind-wave-earthquake loadings as presented in Fig. 2.

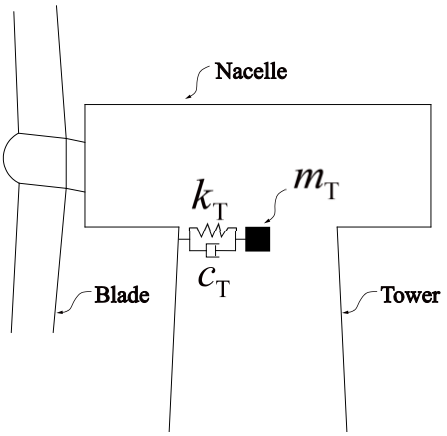

207

208 Fig. 2: Schematic diagram of TMD location

209 The implementation of TMD requires modifications in the modelling of the equation of

motion of the wind turbine in FAST. The force produced due to the motion of the TMD is added into the generalized forces, *i.e.* the right terms in Eq. (1). The TMD force F_{TMD} in each direction is derived as follows:

$$F_{\mathrm{TMD}} = -k_{\mathrm{T}} \cdot x_{\mathrm{TMD}} - c_{\mathrm{T}} \cdot \dot{x}_{\mathrm{TMD}} \tag{4}$$

where x_{TMD} and $\dot{x}_{\mathrm{TMD}}$ are the TMD displacement and velocity, respectively. m_{T}, k_{T} and c_{T} are the mass, stiffness and damping of the TMD, respectively.

The motion of the TMD is influenced by the nacelle dynamics associated with centrifugal force, Euler force and Coriolis force. The TMD acceleration $\ddot{x}_{\mathrm{TMD}}$ can be denoted as follows:

$$\ddot{x}_{\mathrm{TMD}} = -\ddot{x}_{\mathrm{N}} - \omega_{\mathrm{N}} \times (\omega_{\mathrm{N}} \times x_{\mathrm{TMD}}) - \alpha_{\mathrm{N}} \times x_{\mathrm{TMD}} - 2\omega_{\mathrm{N}} \times \dot{x}_{\mathrm{TMD}} - F_{\mathrm{TMD}} / m_{\mathrm{T}} \tag{5}$$

where $\ddot{x}_{\mathrm{N}}$ is the nacelle acceleration. ω_{N} and α_{N} are, respectively, the translational and rotational angular velocities of the nacelle. $\omega_{\mathrm{N}} \times x_{\mathrm{TMD}}$, $\alpha_{\mathrm{N}} \times x_{\mathrm{TMD}}$ and $2\omega_{\mathrm{N}} \times \dot{x}_{\mathrm{TMD}}$ denote the contributions of the centrifugal force, Euler force and Coriolis force, respectively.

2.4 Validation of the SCASCA tool

Fig. 3 presents the flowchart of SCASCA for every time step of an analysis. In every time step, d*t*, of a simulation in SCASCA, the earthquake loads acting on the support structure are calculated based on the input ground motion. The TMD kinematics and kinetics are coupled with the dynamics of the nacelle and support structure when solving the equations of motion of the offshore wind turbine.

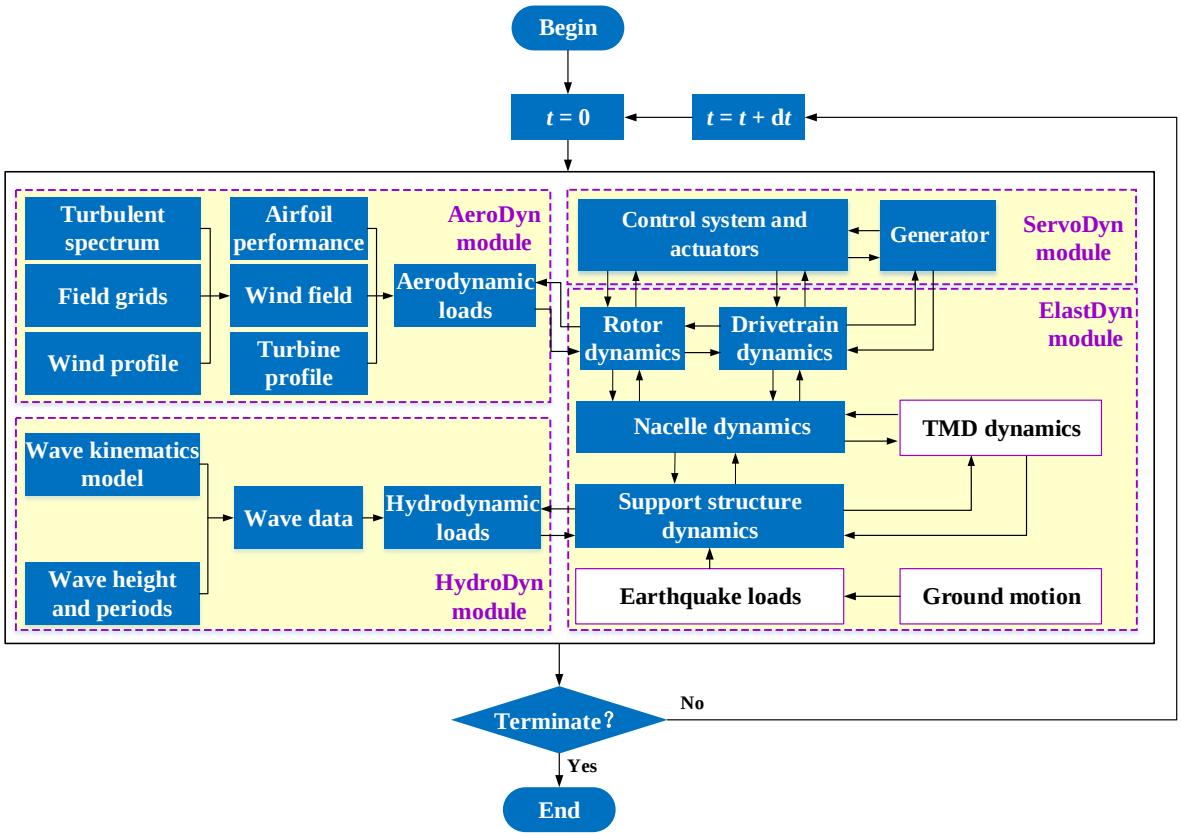

Fig. 3: Flowchart of SCASCA for every time step of an analysis

In order to validate SCASCA, a comparison of the horizontal excitation of an earthquake against Bladed is presented. Fig. 4 presents the tower-top displacements of the NREL 5 MW monopile OWT [23] obtained by Bladed and SCASCA, respectively, for different earthquake loadings. For each of the simulations, the earthquake is assumed to occur at the 20th s. To avoid the influence of the difference between FAST and Bladed in predicting aerodynamic loads, the wind turbine is only subjected to the earthquake loading. As can be seen from Fig. 4, the earthquake-induced responses of the wind turbine calculated by SCASCA agree very well with the results from Bladed for each level of the ground motions. SCASCA efficiently captures the drastic variation of the tower response under an earthquake scenario as confirmed by the agreements between the two numerical analysis tools.

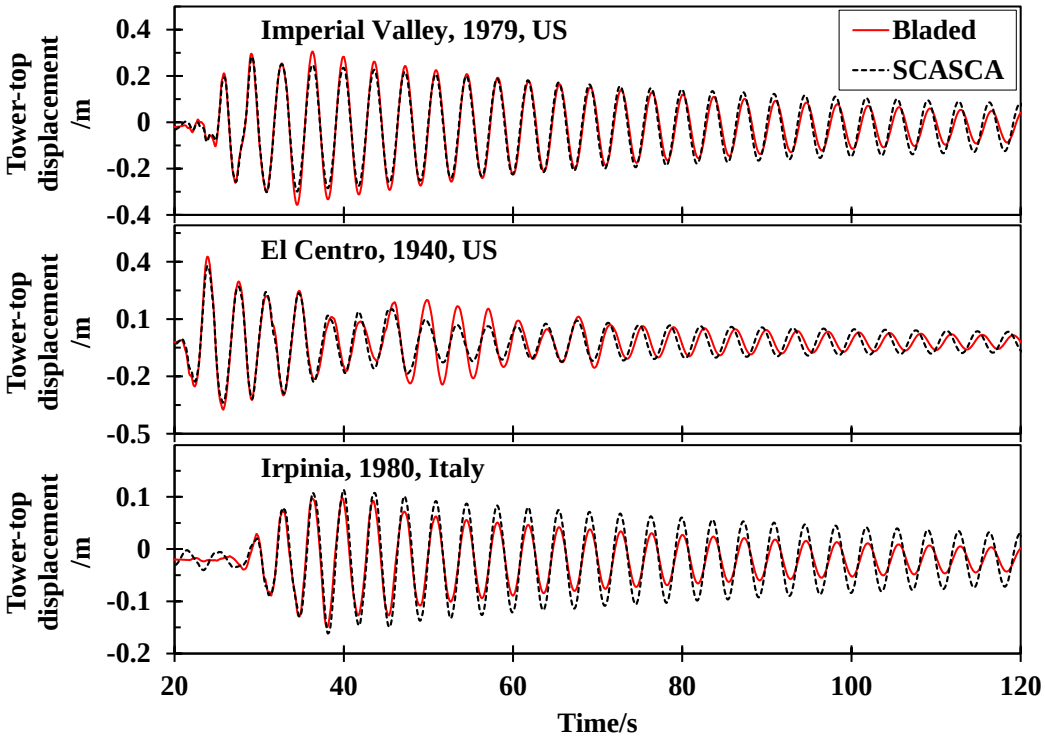

Fig. 4: Comparison of tower-top responses of the NREL 5 MW wind turbine subjected to different ground motions between Bladed and SCASCA

It is noted that SCASCA addresses the limitation of the commonly-used commercial software, Bladed [9], in handling the vertical earthquake excitation. The accuracy of SCASCA in examining the vertical earthquake excitation is validated by comparing it with NREL-Seismic tool that employed the big-mass approach for earthquake load prediction. Fig. 5 presents the tower-base vertical shear-force of the wind turbine under different earthquake loadings. The mass of the fictive platform adopted in NREL-Seismic code is 7.0×10^6 kg, that is the value recommended for the land-based NREL 5 MW wind turbine. As can be seen from Fig. 5, the vertical shear-force at the tower-base predicted by SCASCA follows the same trend with similar magnitudes compared to the results calculated by NREL-Seismic for each of the earthquake events. The result of SCASCA is slightly larger than the result of NREL-Seismic for the Irpinia earthquake record. The minor discrepancy between the results is due to the fact

256 that the fictive platform mass defined in NREL-Seismic program was for the land-based wind
257 turbine, resulting in a relatively smaller prediction of the earthquake load. For the other two
258 earthquake events, the differences between the results of SCASCA and NREL-Seismic are
259 insignificant. The overall agreements between the results are good, indicating that the
260 capability of examining vertical earthquake excitation is well implemented within SCASCA.

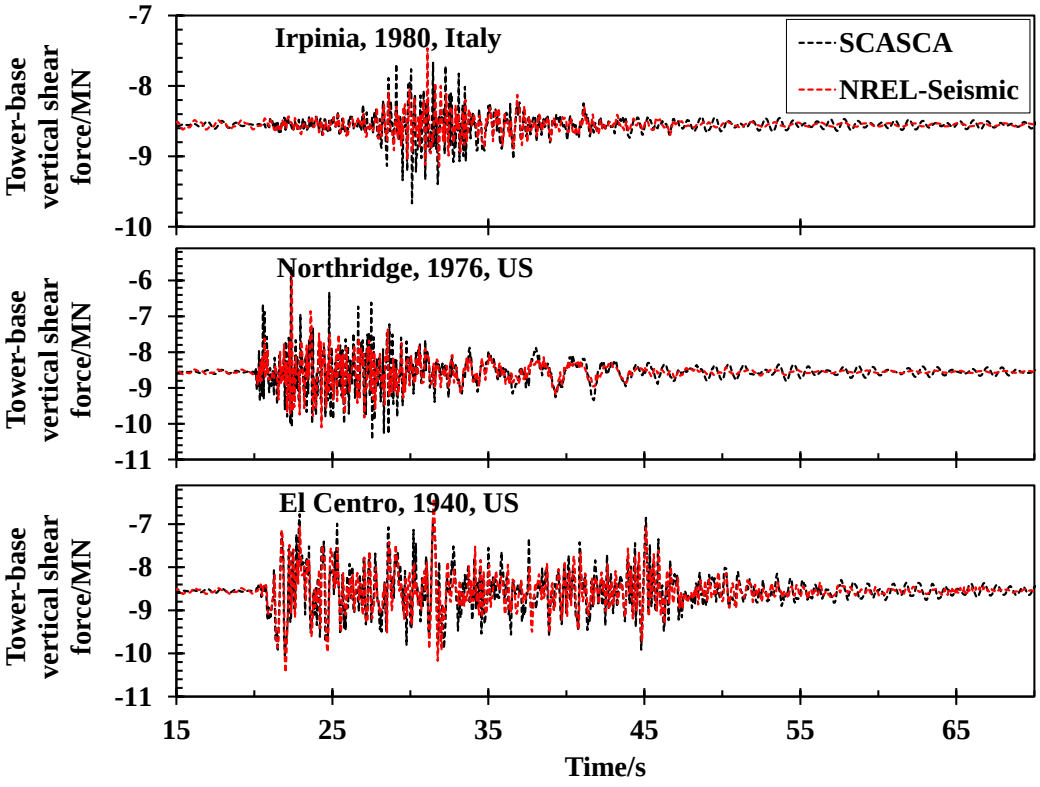

261

262 Fig. 5: Comparison of tower-base vertical shear-force of the NREL 5 MW wind turbine
263 subjected to different vertical ground motions between NREL-Seismic and SCASCA

264

265 The comparisons above verify that SCASCA has a high accuracy in performing seismic
266 analysis of OWTs. Since the linear modal approach is used for the structural modelling, the
267 stiffness of the structures is assumed to remain unchanged under an earthquake event,
268 implying that SCASCA tool is incapable of examining nonlinear material characteristics in
269 the determination of a plastic damage.

3 Numerical modelling of the 10 MW offshore wind turbine

3.1 Design characteristics of the 10 MW monopile wind turbine

The 2012 Light Rotor project carried out in the collaboration between Technical University of Denmark (DTU) and Vestas was aimed at developing a light-weight blade for 10+ MW wind turbines [29]. BECAS and HAWCStab2 were used to conduct the lay-up design and aero-elastic stability analysis of the blades. The DTU reference land-based wind turbine was developed by assembling the blades with other essential structural components including hub, tower and nacelle.

Offshore application of the DTU 10 MW wind turbine requires structural strength enhancements on the support system to guarantee safety and integrity of the entire wind turbine system. Velarde [27] developed four monopiles for the DTU 10 MW wind turbine operating in different water depths (20 m ~ 50 m) by considering the nonlinear SSI effects. The dimensions of the baseline land-based tower were enlarged against more severe offshore environmental loadings. Since monopile type OWTs are more suitable for water depths within 15 m to 30 m, the monopile designed for the 30 m water depth is adopted in this study. The corresponding up-scaling factors for the tower diameter and thickness are 1.25 and 1.3, respectively. The diameter and thickness at tower top are modified to 6.25 m and 35.0 mm, respectively. The diameter and thickness at tower base are changed to 9.00 m and 66.5 mm, respectively. The schematic diagram and a summary of main specifications of the DTU 10 MW monopile OWT are presented in Fig. 6 and Table 1, respectively.

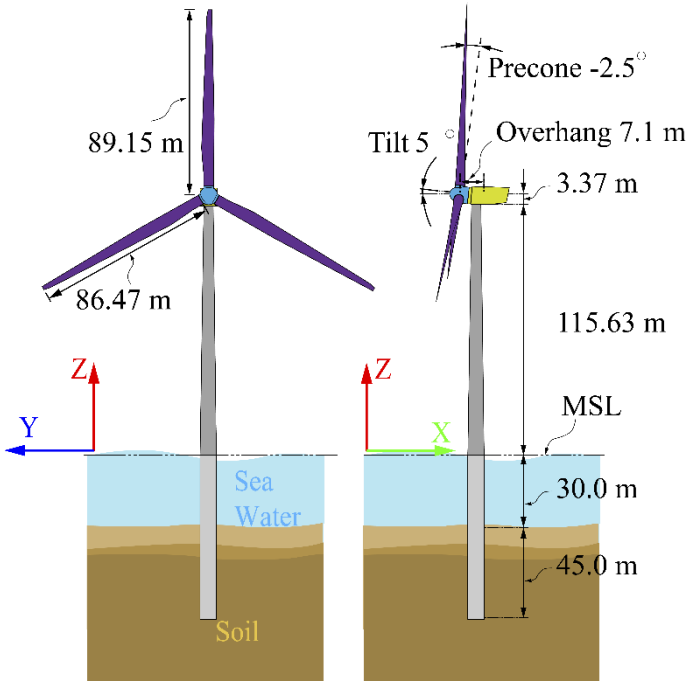

Fig. 6: Schematic diagrams of the DTU 10 MW OWT

Table 1: Main specifications of the DTU 10 MW OWT

Specification (Unit)	Value	Specification (Unit)	Value
Rated power (MW)	10.0	Nacelle mass (kg)	4.46×10^5
Cut-in/cut-out speeds (m/s)	4/25	Tower mass (kg)	1.20×10^6
Rated wind speed (m/)	11.4	Tower height (m)	115.63
Cut-in/rated rotor speeds (rpm)	6/9.6	Tower top diameter (m)	6.25
Rotor diameter (m)	178.3	Tower base diameter (m)	9.0
Hub diameter (m)	5.6	Tower top thickness (mm)	35.0
Gear box ratio(-)	50	Tower base thickness (mm)	66.5
Shaft tilt angle (°)	5.0	Monopile diameter (m)	9.0
Hub height (m)	119.0	Monopile thickness (mm)	110.0
Rotor mass (kg)	227,962	Monopile length (m)	75
Blade pre-cone angle (°)	-2.5	Monopile mass (kg)	1.96×10^6

3.2 Modelling of soil-structure interaction (SSI) effects

The selected site of the wind turbine has a single soil layer of sand with a saturated soil weight of 20 kN/m^3 and an internal friction angle of 36°. The pile-soil interaction is

represented by the Winkler spring-dashpot model [24**Error! Bookmark not defined.**] to consider the soil effect. The stiffness of each spring is derived by force-displacement relationships (*p-y* curves). By applying different cyclic loads at the mudline of the monopile, the *p-y* curves along the embedded length of the monopile were obtained using the finite element software Plaxis 3D. Regarding the soil damping due to radiation and hysteretic effects, the model developed by Gazetas *et al.* [30] is used to determine the soil damping as follows:

$$C_s = 6\sqrt{\rho_s G_s} D_m \left(\frac{\omega_m D_m}{\sqrt{G_s/\rho_s}}\right)^{-1/4} + 2\beta_s \frac{k_s}{\omega_m} \tag{6}$$

where C_s is the soil damping; ρ_s and G_s are the density and shear modulus of the soil, respectively. D_m is the monopile diameter. ω_m is the 1st-order natural angular frequency of the support structure. k_s is the stiffness derived from the *p-y* curves and β_s is the hysteresis damping ratio with a value of 5%.

The stiffness and damping distributions along the embedded pile subjected to a lateral force of 30 MN are presented in Fig. 7. The stiffness close to the seabed level is about two orders lower than that at the bottom of the monopile. The soil reaction F_s due to relative displacement d_s and velocity v_s between the soil and monopile under external loadings is given as:

$$F_s = -k_s \cdot d_s - C_s \cdot v_s \tag{7}$$

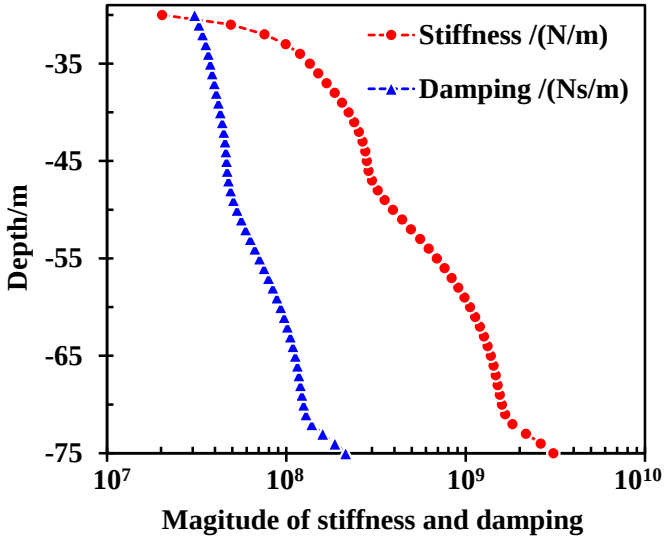

Fig. 7: Linear stiffness and damping of the Winkler spring-dashpot model of the 30 m water depth monopile

4 Seismic behaviour of the 10 MW wind turbine

4.1 Scaling of the ground motion

The monopile used in this study was designed for a typical medium-stiff soil with an internal friction angle of 36°. The saturated and effective unit weight of the soil are 20 kN/m^3 and 17 kN/m^3, respectively. In order to be consistent with the design of the monopile, a medium-stiff site in the eastern coast of China is chosen for the case study of the 10 MW monopile OWT.

The ground motion recorded in the 1979 Imperial Valley earthquake event is chosen as the input earthquake acceleration. In order to ensure that the frequency contents of the selected ground motion is consistent with the geological characteristics of the specific area, the response spectrum of the ground motion is modified to match a target response spectrum

that is defined in accordance with the seismic design code. Fig. 8 presents a seismic response spectrum with a design acceleration of 0.40 g and a damping ratio of 5 % defined in accordance with the Chinese code for seismic design of buildings [31]. T_g is a site depended characteristic parameter that denotes the ratio between the design spectral acceleration ($a_{\max}$) and the spectral acceleration at 1.0 s. According to the Chinese seismic design code, the value of T_g is chosen as 0.43 s for a medium-stiff site in the eastern coastal areas of China. For the ninth-level seismic design intensity, the longitudinal design acceleration is chosen as 0.40 g. The ratio between the design acceleration magnitudes of the longitudinal and lateral ground motions is 1:0.85. The target response spectra corresponding to the horizontal ground motions are obtained accordingly.

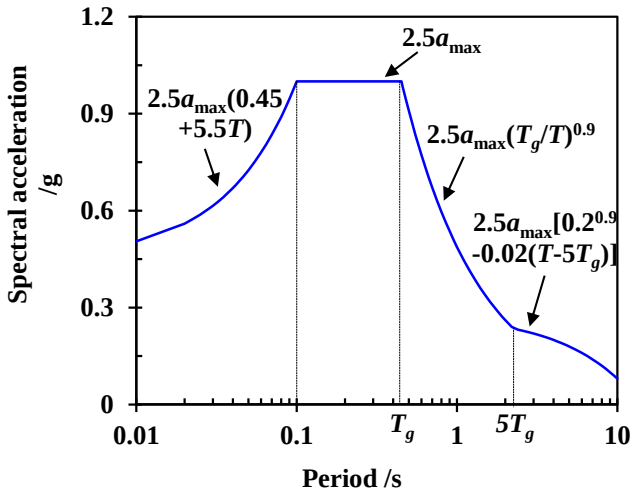

Fig. 8: Target response spectrum for a China's eastern coastal site

The application of the ground motion scaling is to eliminate the spectral misfits between the initial and the target response spectra. The scaling of the longitudinal and lateral ground motions is conducted using the "RspMatch" code developed by Atik *et al*. [32]. In the scaling process, different wavelet components are iteratively added into the initial earthquake record

346 to adjust its frequency characteristics until the spectral misfit to the target spectrum falls
347 below a given tolerance value. Fig. 9 presents the response spectra and accelerograms of the
348 initial and adjusted ground motions. The initial response spectrum is the spectral acceleration
349 of the 1979 Imperial Valley earthquake recorded by El Centro Array #6 station. The adjusted
350 response spectrum corresponds to the earthquake acceleogram modified by the "RspMatch"
351 code in the scaling process.

352 From Fig. 9-(a) and Fig. 9-(b), it is observed that the response spectrum of the adjusted
353 ground motion in each of the horizontal directions agrees very well with the target spectrum.
354 It means that the adjusted ground motion is capable of representing the earthquakes in the
355 target site. The accelerograms indicate that the peak of ground acceleration (PGA) of the
356 adjusted ground motion in the longitudinal direction is around 0.40 g. This means that the
357 adjusted ground motion has satisfied the requirement of the scaling process.

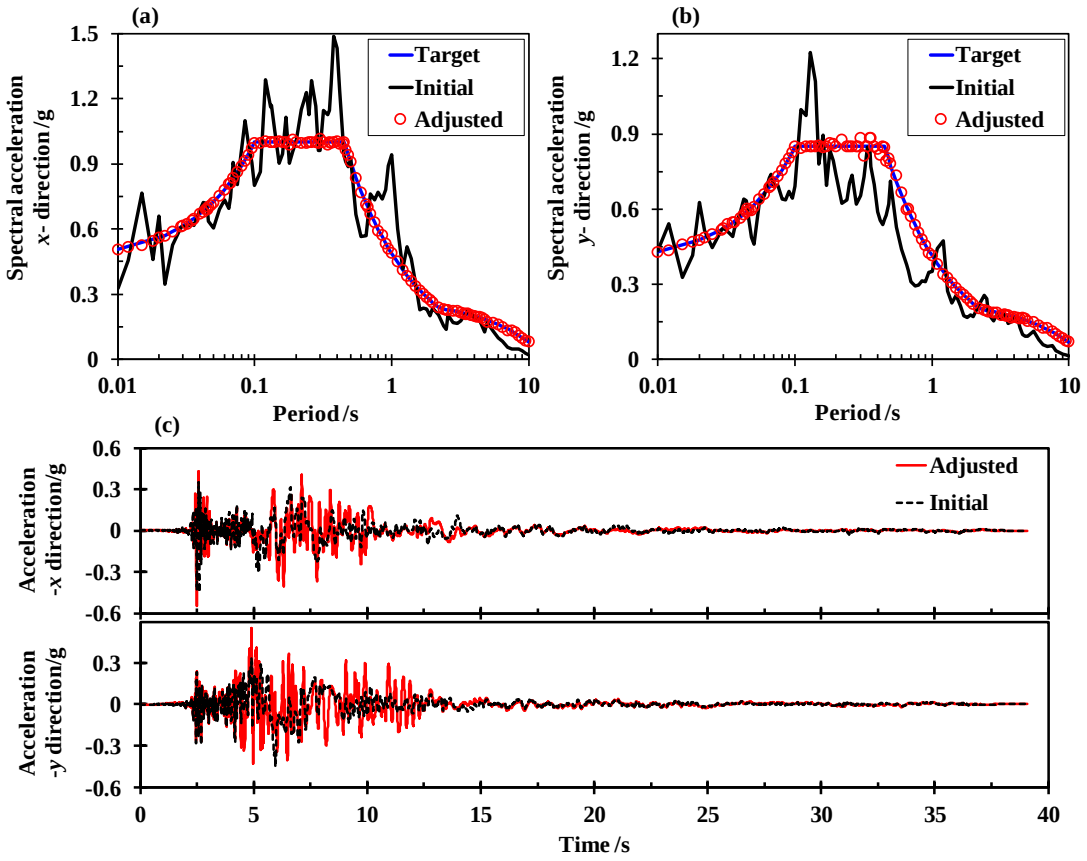

Fig. 9: Response spectra and accelerograms of the initial and adjusted ground motions in the longitudinal (*x*-aligned with wind and wave) and lateral (*y*) directions

4.2 Coupled responses due to wind-wave-earthquake loadings

In order to evaluate the contribution of the earthquake loading to the coupled responses of the 10 MW OWT, three different loading scenarios examined in this study are presented in Table 2. The wave direction is assumed to be aligned with the inflow direction of the wind.

Table 2: Loading scenarios for the simulations

Load cases	Wind speed (m/s)	Wave height (m)	Wave period (s)	Earthquake (-)
Earthquake-only	(-)	(-)	(-)	Imperial Valley
Wind-wave-only	11.4	6.0	12.5	-
Coupled-loading	11.4	6.0	12.5	Imperial Valley

The full-field turbulent wind is generated using TurbSim [33] based on the Kaimal spectrum. Fig. 10 presents the wind speeds at the hub height. The spatial and time-domain variations of the wind speed have confirmed the turbulent features of the generated wind field.

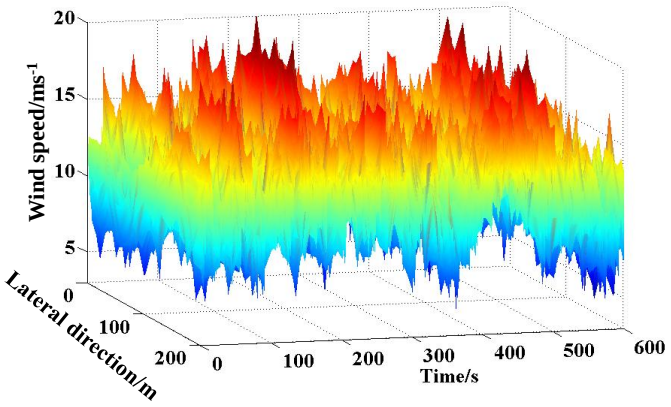

Fig. 10: Wind speed at the hub height

The baseline FAST is only capable of generating linear waves based on Airy wave theory but accepts user-defined waves in a specific format. In order to consider nonlinearity of the waves, the kinematics of the nonlinear waves are reproduced based on the third-order Stokes wave theory [34]. Fig. 11 presents the wave kinematics versus depth.

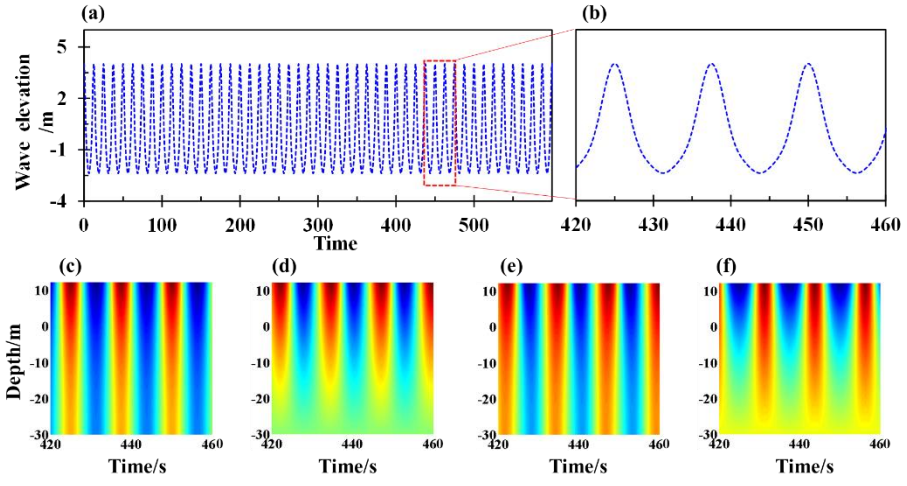

Fig. 11: Wave elevation and kinematics of the nonlinear wave. (a) wave elevation; (b) enlarged vision of wave elevation; (c) longitudinal velocity; (d) vertical velocity; (e)

longitudinal acceleration; (f) vertical acceleration

Each of the simulations has a duration of 600 s and a time step of 0.002 s. The earthquake excitation is added at the 400th s to avoid the influence of the transient behaviour of the wind turbine. Fig. 12 presents a comparison of the tower-top displacements of the 10 MW monopile OWT under the three loading scenarios.

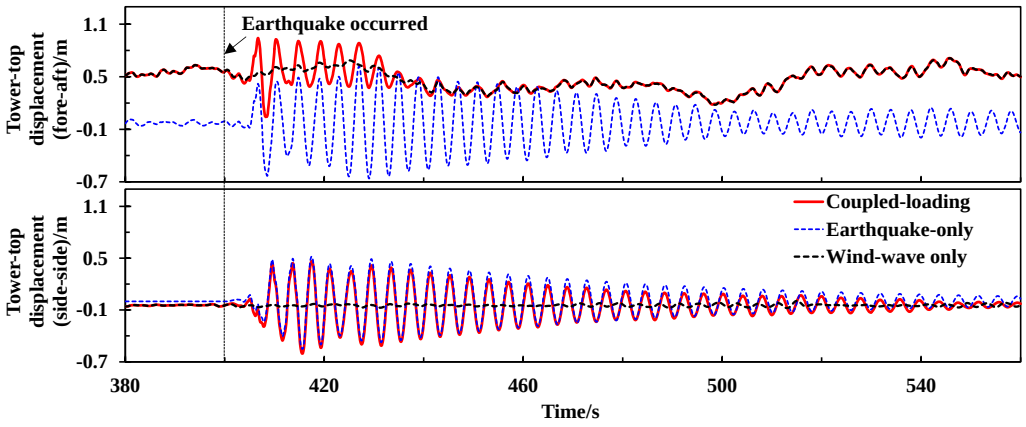

Fig. 12: Tower-top displacement time series of the 10 MW OWT subjected to different loading combinations

For the earthquake-only scenario, both the tower-top's fore-aft and side-side displacements fluctuate periodically with large amplitude after the earthquake occurred. The variation ranges of the tower-top's fore-aft and side-side displacement are -0.66 m~0.62 m and -0.55 m~0.52 m, respectively. The tower vibrates more severely in the fore-aft direction due to the stronger component of the ground motion. After the high intensity excitation (>440 s), the tower-top displacements start to decay. The decay ratio of the fore-aft tower-top displacement under the earthquake-only condition is smaller than that of the coupled-loading condition. Moreover, the fore-aft tower-top displacement resulted from the coupled-loading varies within the range of 0.04 m to 0.94 m. This is comparatively smaller than the variation

range corresponding to the earthquake-only condition. The observations indicate that the tower vibration in the fore-aft direction is mitigated by the wind and wave loadings. The reason behind this is that the presences of wind and wave provide aerodynamic and hydrodynamic damping for dissipating the energy from the earthquake excitation. The fore-aft tower-top displacement fluctuates within the range of 0.48 m to 0.71 m when the wind turbine operates under the wind-wave-only condition. The fluctuation over the simulation is much smaller than that of the other two loading scenarios. This implies that the vibration induced by the wind and wave is much less severe compared to the vibration caused by the earthquake, although the average displacement contributed by the elastic deformation is higher.

The spectral curves of the tower-top accelerations of the 10 MW monopile OWT under the three loading scenarios are obtained using the Welch spectrum method and are presented in Fig. 13.

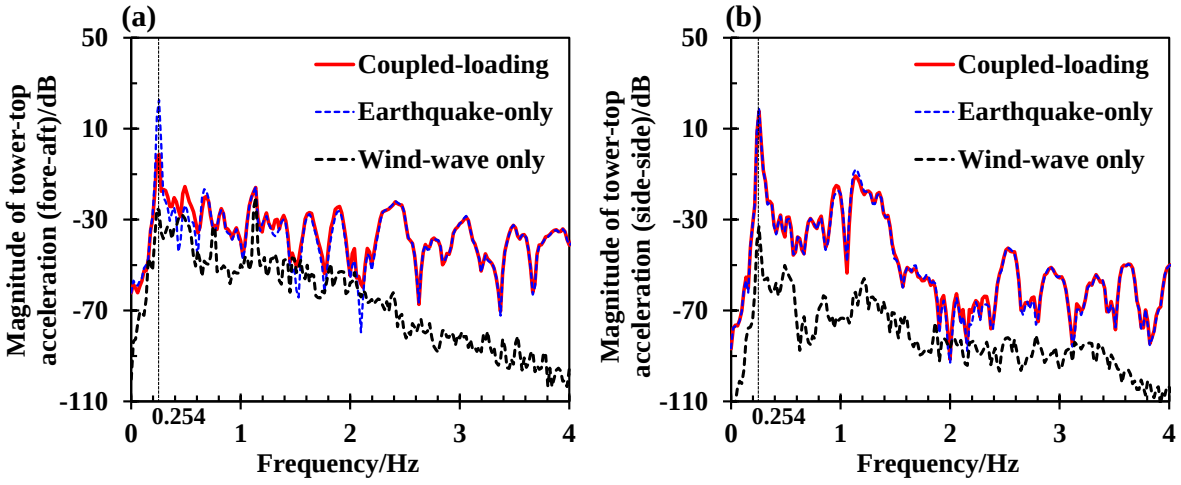

Fig. 13: Welch spectral curves of the tower-top accelerations of the 10 MW OWT under different loading scenarios for: (a) fore-aft direction and (b) side-side direction.

The first-order natural mode of the support structure is the main contributor to the

tower-top vibration for both the fore-aft and side-side directions as confirmed by the peak magnitude presence at 0.254 Hz. It is noted that the fore-aft magnitude of the coupled-loading condition is much lower than that of the earthquake-only scenario. This further confirms that wind and wave loadings have positive effects in mitigating the earthquake-induced vibration. Due to the absence of wind in the side-side direction, the peak magnitudes at the first-order natural frequency of the support structure agree well between the coupled-loading and earthquake-only conditions. In addition, the spectral magnitudes of the tower-top acceleration from the wind-wave condition are significantly smaller than those from the remaining two loading conditions. This observation confirms that the earthquake is the dominant loading of the tower vibration.

Fig. 14 presents the maximum resultant displacement and bending moment along the support structure elevation for the three examined loading conditions. The tower-top displacement resulting from the earthquake-only condition is slightly larger than that of the wind-wave condition. This implies that the magnitude of the tower vibration caused by the earthquake excitation is larger than the elastic deformation due to the wind-wave loading. The tower-top displacement resulting from the coupled-loading exceeds 1.0 m, which is much larger than the values of the other two loading scenarios. Compared with the wind-wave condition, the earthquake enhances the tower-top displacement by 47.6% and the pile-cap bending moment by 95.1%。

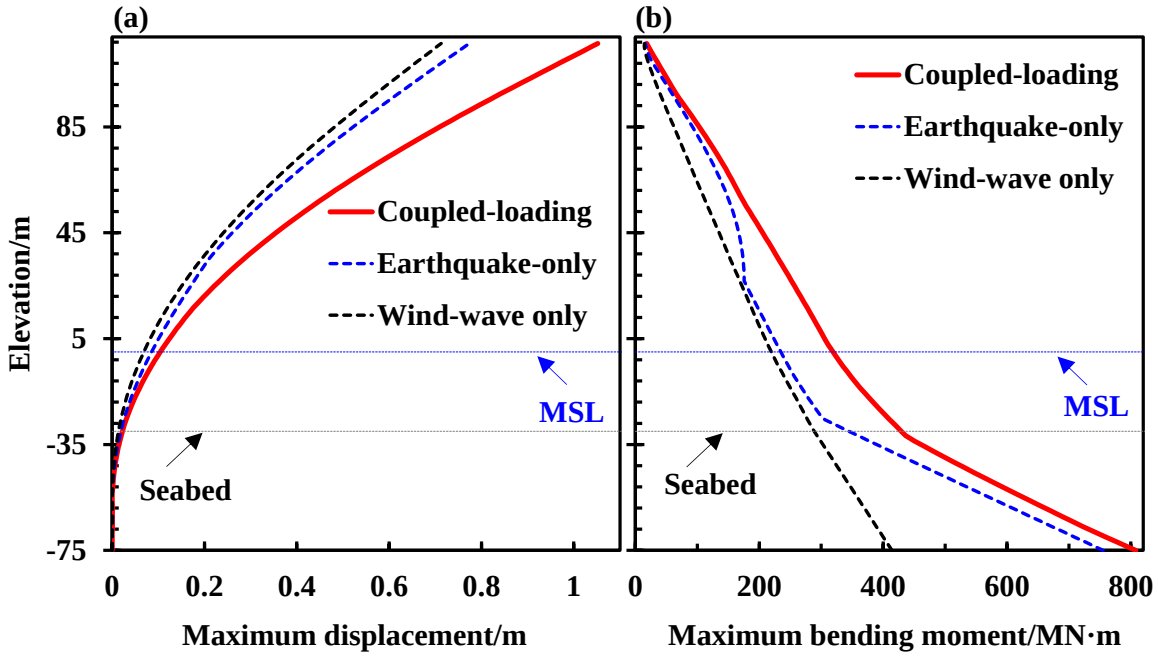

435

436 Fig. 14: Maximum responses along the support structure elevation of the three examined

437 loading scenarios: (a) displacement and (b) bending moment

438

439 The maximum tower bending moment due to wind-wave condition increases linearly

440 with the support structure elevation, which is significantly different from the variation trend

441 corresponding to an earthquake event. The tower bending moment varies more severely with

442 the elevation of the embedded portion when the wind turbine is subjected to the earthquake

443 loading. For an arbitrary elevation, the bending moment of the support structure under the

444 earthquake-only condition is slightly larger than that of the wind-wave condition. This

445 indicates that the earthquake loading is the dominant excitation of the OWT. The maximum

446 bending moments of the support structure at the seabed and pile-cap locations under the

447 coupled-loading condition are 428 MN·m and 808 MN·m, respectively. For the wind-wave

448 scenario, the bending moments at the seabed and pile-cap are 288 MN·m and 414 MN·m,

449 respectively. The earthquake enhances the loads by 48.7% and 95.1%, respectively. It means

450 that the monopile beneath the seabed suffers much stronger loads compared to the portion
451 above the ground. It is noted that the thickness of the monopile remains unchanged for the
452 embedded portion in the original design [24]. The results obtained in this study suggest that
453 the monopile thickness should increase with soil depth for the seismic resistance design of
454 wind turbines operating in earthquake-prone sites.
455

456 # 5 Mitigation control using TMDs

457 The previous results have indicated that the earthquake loading significantly enhances
458 tower vibration and bending moment of the OWT. In order to reduce the risk of structural
459 damage potentially caused by earthquake loadings, TMD is employed to mitigate the tower
460 vibration and loads on the 10 MW monopile OWT under an earthquake event.

461 ## *5.1 Sensitivity of control parameters*

462 For the TMD with a mass, m_{T}, and a stiffness, k_{T}, the tuned frequency f_{T} can be
463 denoted as:

464 $$f_{\mathrm{T}}=\sqrt{k_{\mathrm{T}}/(m_{\mathrm{T}}\cdot 4\pi^2)} \tag{8}$$

465 The mass and first-order natural frequency of the 10 MW OWT are m_{WT} and f_{WT},
466 respectively. The tuned frequency ratio λ and mass ratio μ are defined as follows:

467 $$\begin{cases}\lambda = f_{\mathrm{T}}/f_{\mathrm{WT}} \\ \mu = m_{\mathrm{T}}/m_{\mathrm{WT}}\end{cases} \tag{9}$$

468 The mitigation effect on the seismic behaviour of the wind turbine is sensitive to the
469 control parameters including the tuned frequency and damping of a TMD. To obtain the best
470 mitigation effect, a sensitivity analysis of the control parameters is performed for the

earthquake-only condition. Fig. 15 presents the maximum tower-top displacement of the OWT under the control of a 5% mass ratio TMD with different tuned parameters. The maximum tower-top displacement of the OWT without the TMD is 0.76 m. All the examined TMDs are effective in reducing the tower-top displacement as can be observed from Fig. 15. The mitigation effect is sensitive to the damping ratio for the frequency ratio within the range from 0.88 to 1.1. A higher damping ratio leads to a relatively larger reduction of tower-top displacement. The mitigation effect of the TMD is more sensitive on the frequency ratio. The tower-top displacement decreases significantly with decrease in the frequency ratio. The TMD with a frequency ratio lower than 0.85 has similar mitigation effects on the tower-top displacement. The largest mitigation is achieved at 42.5% by using the TMD with a frequency ratio of 0.87 and a damping ratio of 0.12.

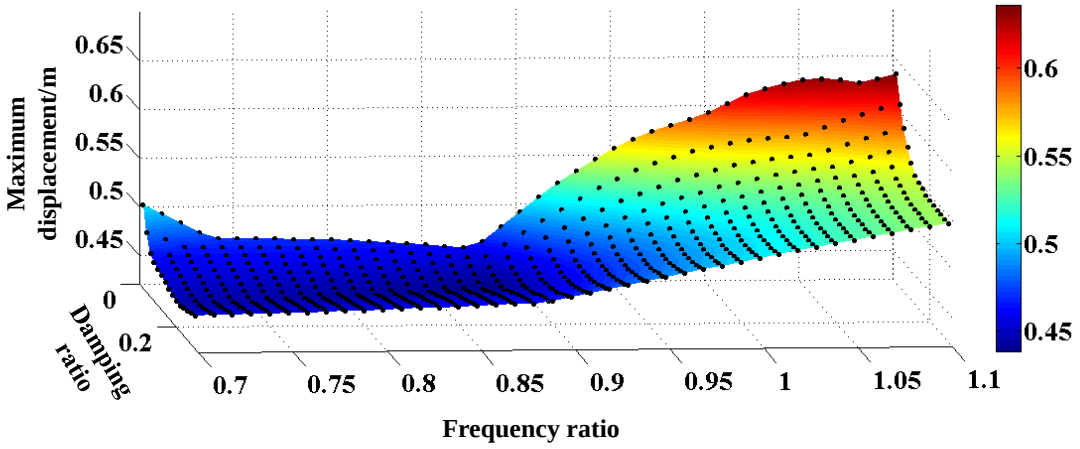

Fig. 15: Tower-top displacement versus frequency and damping ratios of TMDs

Fig. 16 presents the tower-top displacements of the OWT under the control of an optimal TMD against an ordinary TMD for the coupled-loading condition. Both of the TMDs are effective in reducing the peak of the fore-aft tower-top displacement. The TMDs accelerate the decay process to a more stable level after the strong ground motion (>410 s). It is noted that the tower-top displacement over the simulation of the optimal TMD scenario is smaller

compared to the ordinary TMD with a frequency ratio of 1.0 and a damping ratio of 0.1. The tower-top trajectories imply that the tower vibrates in a smaller range under the control of the optimal TMD. The observations indicate that the optimal TMD can better alleviate the earthquake-induced responses compared to the ordinary TMD.

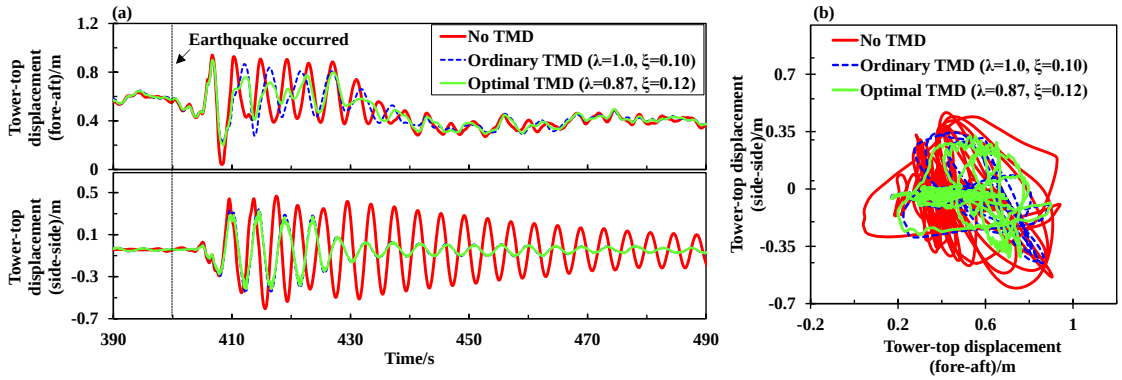

Fig. 16: Tower-top displacements of the coupled-loading scenario: (a) time-domain variation and (b) tower-top trajectory

The tower-top displacements under the earthquake-only condition for different TMD configurations are presented in Fig. 17. The fluctuations of the tower-top displacements in both fore-aft and side-side directions are significantly mitigated by the TMDs. The standard deviations of the fore-aft and side-side tower-top displacements are reduced by 70.4% and 56.8 % respectively. Similar to the results of the coupled-loading scenario, the optimal TMD is more efficient in eliminating the fluctuation of the tower-top displacement caused by the earthquake, resulting in a narrower range of the tower-top motion trajectory.

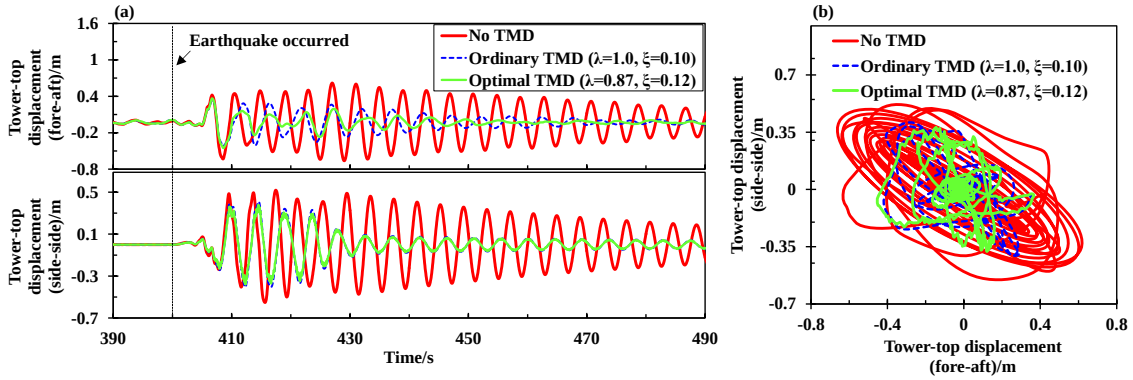

504

505 Fig. 17: Tower-top displacements of the earthquake-only scenario: (a) time-domain variation

506 and (b) tower-top trajectory

507

508 ## *5.2 Effects of mass ratio on response mitigation*

509 Mitigation of the dynamic responses of the wind turbine subjected to an earthquake

510 excitation is also affected by the mass ratio of the TMD. In order to investigate the influence

511 of the mass ratio with respect to the mitigation effect, sensitivity analysis of the frequency and

512 damping ratios is performed on the TMDs with different mass ratios. The optimal frequency

513 and damping ratios corresponding to different mass ratios are presented in Fig. 18. The linear

514 fitted lines of frequency and damping ratios can be used to obtain the optimal control

515 parameters corresponding to an arbitrary mass ratio without performing numerous parametric

516 analysis.

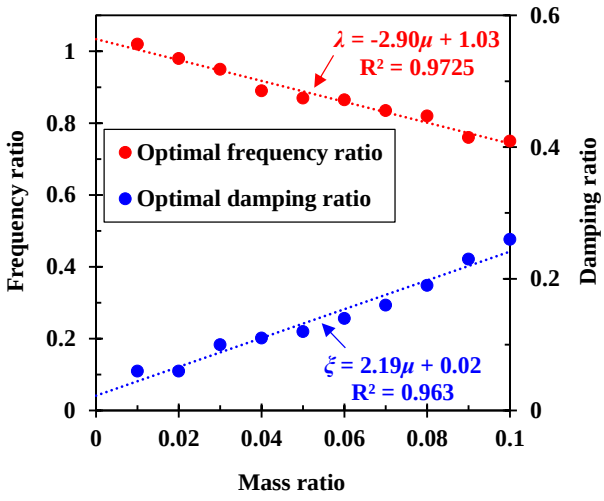

Fig. 18: Optimal frequency ratio and damping ratio versus mass ratio

It is noted that the optimal frequency ratio decreases with increase in the mass ratio, which is opposed to the variation trend of the optimal damping ratio. This is because the TMD located at the tower-top affects the natural frequency of the wind turbine system, which decreases with increase in the TMD mass. The mitigation of structural responses is achieved only when the tuned frequency of the TMD is close to the natural frequency of the OWT. Therefore, a smaller tuned frequency is required to obtain the best mitigation effectiveness for a heavier TMD.

Fig. 19 presents the mitigation effect of the TMDs with different mass ratios for both the coupled-loading and earthquake-only scenarios. For the coupled-loading scenario, the reduction in the maximum tower-top displacement increases with the mass ratio. The maximum tower-top displacement can be reduced by over 10% if the mass ratio of the TMD is larger than 0.01. It is noted that the alleviation effect of the TMD is insignificant when the mass ratio is larger than 0.06. The same observation can be made for the earthquake-only condition. In addition, the TMD with a mass ratio of 0.05 is able to reduce the maximum

tower-top displacement by 39%, implying that TMD has much better effect on reducing the tower displacement for the earthquake-only condition. The reason is that the TMD is effective in mitigating tower vibration caused by an earthquake, and it is not capable of reducing the tower elastic deformation which is the major contribution of tower displacement for the coupled-loading condition.

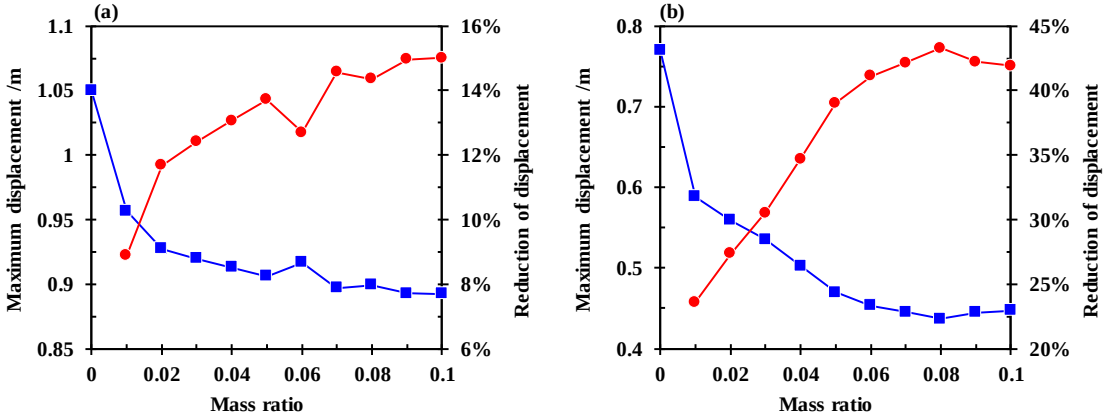

Fig. 19: Optimal control parameters of the TMDs with different mass ratios. (a) coupled-loading and (b) earthquake-only condition

Fig. 20 presents the tower-top displacement variations of the OWT under the control of different optimal TMDs. Although the TMD with a mass ratio of 0.07 leads to a smaller resultant tower-top displacement, the TMD with a mass ratio of 0.05 can better alleviate the vibration in the side-side direction for both examined loading cases. The results indicate that the TMD with a lower mass ratio could be a better option.

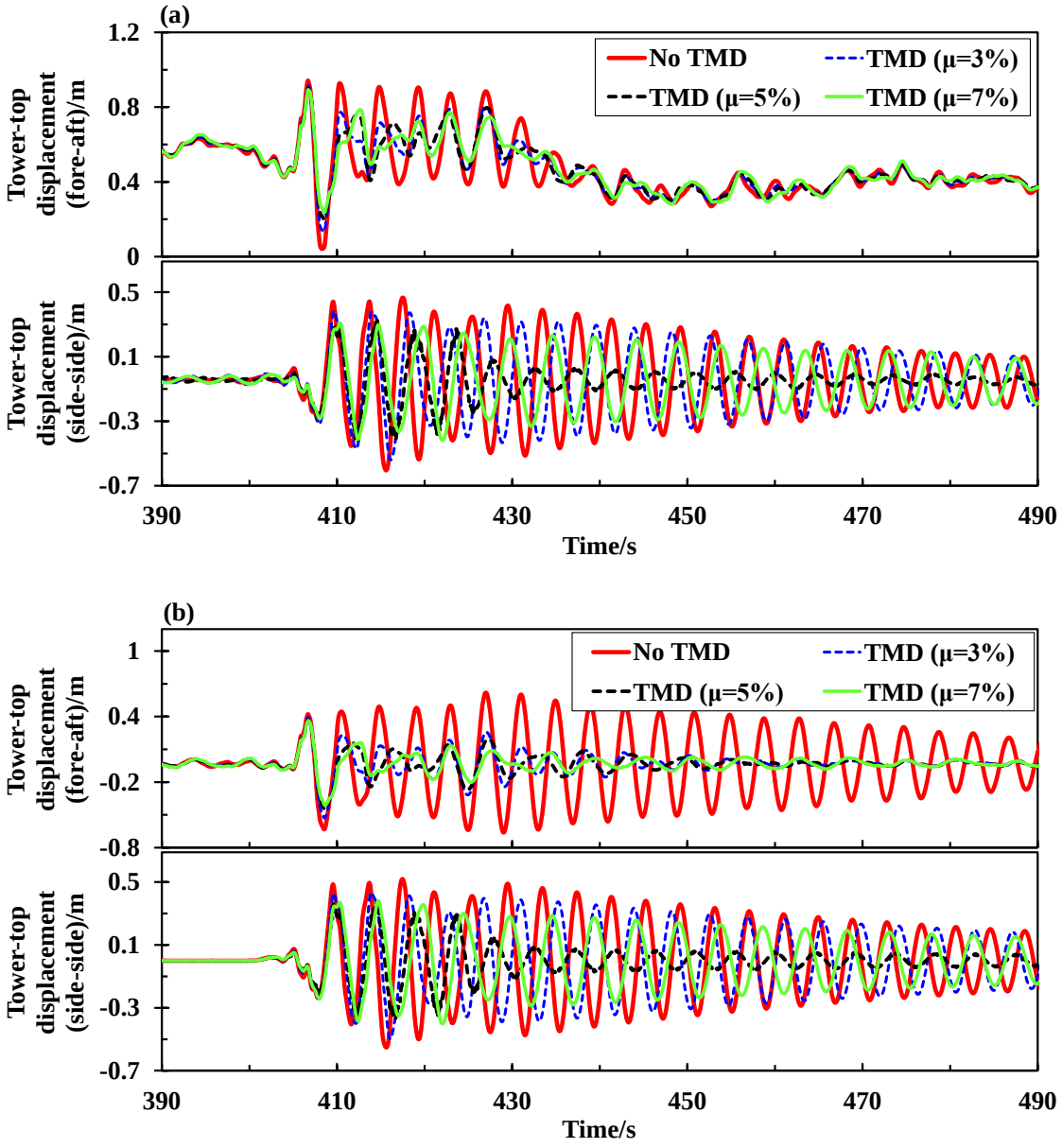

548

549

550 Fig. 20: Comparison between tower-top displacements controlled by different TMDs for (a)

551 coupled-loading and (b) earthquake-only scenarios

552

553 Fig. 21 presents the spectral curves of the tower-top displacement of the 10 MW OWT

554 for different optimal TMDs under the earthquake-only condition. The magnitude of the

555 fore-aft tower-top displacement at the 1st-order natural frequency (0.254 Hz) has been reduced

556 significantly by the TMDs. It is also noted that the vibration frequency decreases with the

increase in the TMD mass ratio. This further confirms the conclusion that a heavier TMD requires lower tuned frequency for the best mitigation effect. The TMDs have comparatively insignificant effect in mitigating the vibration of the side-side direction. Nonetheless, the peak magnitude of the TMD with a mass ratio of 0.05 is reduced significantly as the fore-aft displacement. This implies that the 0.05 mass ratio TMD is the optimum configuration for use in the mitigation control of the 10 MW OWT in earthquake-prone areas.

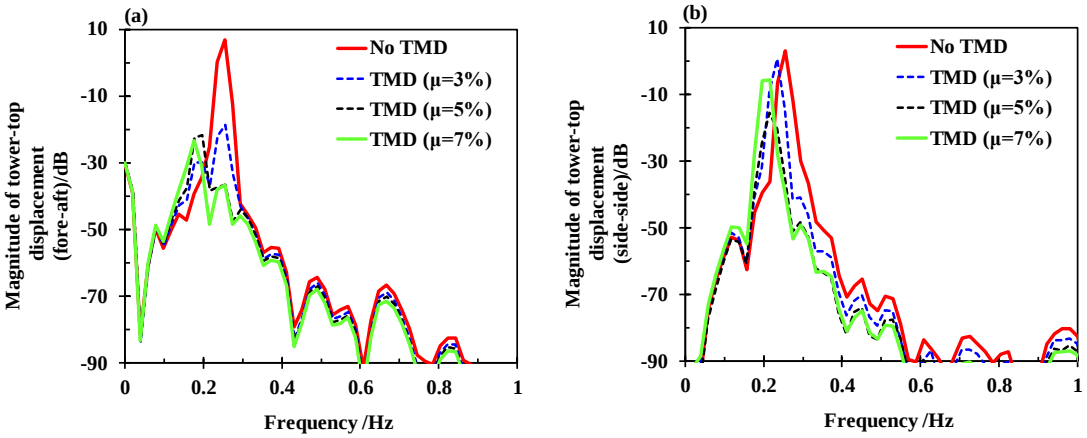

Fig. 21: Magnitude of tower-top displacements of the (a) fore-aft and (b) side-side directions in frequency domain for the earthquake-only condition

6 Discussions

The results of the coupled-loading condition indicate that the earthquake excitation increases the tower-top displacements in the fore-aft and side-side directions. An interesting observation is that the spectral magnitude of the fore-aft tower-top displacement at the first-order natural frequency under the coupled-loading condition is much smaller than that of the earthquake-only condition. It means that aerodynamic load is effective in mitigating the earthquake-induced vibration. The explanation to this result is that the interaction between

rotor and wind dissipates the energy from the earthquake excitation. The presence of aerodynamic damping has positive effect in alleviating the tower vibration under an earthquake event. Moreover, it is noted that the monopile beneath the seabed suffers much stronger loads compared to the portion above the ground when the earthquake excitation is examined. However, this observation was not present in the wind-wave condition. This is attributed to the fact that there is only soil reaction force acting on the monopile beneath the seabed in the wind-wave-only condition. But when the earthquake loading is considered, the earthquake excitation makes significant contribution to the loads on the embedded monopile. As a result, the slope of the bending moment varying with the monopile elevation is significantly increased.

The results of the structural control analysis indicate that a TMD with rational parameters is efficient in mitigating the tower vibration. The coupling between the dynamics of the TMD and tower results in smaller tower responses, since the TMD dissipates energy from the external excitations. The results also show that a heavier TMD with a smaller tuned frequency is capable of achieving a larger mitigation on the tower responses. An explanation to this observation is that a heavier TMD can dissipate more energy from the wind turbine system. It is noted that the vibration mitigation is achieved only when the tuned frequency of the TMD is close to the natural frequency of the wind turbine system which decreases with the increase of TMD mass. This explanation is further confirmed by the spectral results of the tower-top responses where the peak spectral magnitude corresponds to a lower frequency for a heavier TMD.

7 Conclusions

This study investigates the use of TMD for the mitigation of the coupled responses of a 10 MW monopile OWT due to wind, wave and earthquake loadings. A generic tool, SCASCA, has been developed to examine the coupling effects of multiple loadings. The comparisons of the tool's outputs against Bladed and NREL-Seismic have validated the accuracy and capability of SCASCA in performing fully coupled seismic analysis of OWTs. Furthermore, SCASCA is also capable of performing structural control analysis using TMDs. The effect of TMDs in mitigating the dynamic responses of the 10 MW monopile OWT subjected to a scaled ground motion is investigated. This study offers the following conclusions:

(1) Comparisons of SCASCA's results against Bladed and NREL-Seismic have validated its accuracy and capability in performing fully coupled seismic analysis. The generic SCASCA is independent of the user's experience compared to FAST-Seismic for design of different wind turbines. In addition, SCASCA addresses the limitation of FAST-Seismic in considering the SSI effect and the limitation of Bladed in examining the vertical earthquake excitation.

(2) Coupled responses of the 10 MW OWT due to wind, wave and earthquake loadings are investigated while the SSI effect is examined using the nonlinear *p-y* curves. The earthquake-induced vibration in the fore-aft direction is mitigated by the wind and wave loadings due to the energy dissipation by aerodynamic and hydrodynamic damping. The spectral magnitude at the first-order natural frequency of the fore-aft tower-top displacement is mitigated from 22.6 dB to -20.4 dB. In addition, the tower vibration is dominated by the earthquake as indicated by the Welch spectral results.

(3) The tower-top displacement and pile-cap bending moment increase, respectively, by 47.6% and 95.1% due to the earthquake loading mainly. The bending moment along the embedded pile increases significantly with the soil depth, suggesting that the structural strength of the embedded portion shall be enhanced against earthquake events.

(4) The TMD with appropriate control parameters is effective in mitigating the tower-top displacements for both the coupled-loading and earthquake-only conditions. The standard deviations of the fore-aft and side-side tower-top displacements are reduced by 70.4% and 56.8 % respectively for earthquake-only conditions. The large fluctuations caused by an earthquake can be eliminated efficiently by the TMDs when the design parameters are appropriately selected.

(5) Rational control parameters corresponding to different mass ratios of the TMD are obtained by conducting a sensitivity analysis. It is noted that a heavier TMD requires a lower tuned frequency to achieve a larger mitigation. The 0.05 mass ratio TMD mitigates the maximum tower-top displacement by 13.7% and 39.0% for the coupled-loading and earthquake-only conditions, respectively. The vibration magnitude corresponding to the 1^{st}-order natural frequency is reduced significantly for both of the fore-aft and side-side directions. The 0.05 mass ratio TMD is the recommended configuration for use in the mitigation control of the 10 MW monopile OWT in earthquake-prone areas.

Acknowledgements

The authors would like to acknowledge the financial support from the National Natural Science Foundation of China (grant numbers: 51676131, 51811530315 and 51976131),

Science and Technology Commission of Shanghai Municipality (grant number: 1906052200) and Royal Society (grant number: IEC\NSFC\170054). This study is partially supported by the European Union's Horizon 2020 research and innovation programme under the Marie Skłodowska-Curie grant agreement no. 730888 (RESET) and European Regional Development Fund (ERDF), Interreg Atlantic Area (grant number: EAPA_344/2016).

Nomenclature

DOF	Degree of Freedom
DTU	Technical University of Denmark
EUR	Currency of the European Union
IEA	International Energy Agency
IRENA	International Renewable Energy Agency
LCoE	Levelised Cost of Electricity
NREL	National Renewable Energy Laboratory
OWT	Offshore Wind Turbine
PGA	Peak of Ground Acceleration
RNA	Rotor-Nacelle-Assembly
SCASCA	Seismic Coupled Analysis and Structural Control Architecture
SDG	Sustainable Development Goal
SSI	Soil-Structure Interaction
TMD	Tuned Mass Damper
a_{eq}	Earthquake acceleration
C_s	Soil damping
c_{T}	TMD damping
D_m	Diameter of the monopile
d_s	Structure displacement for soil force calculation
f_{T}	Tuned frequency of the TMD
f_{WT}	Dominant vibration frequency of the wind turbine
$F_{aero,i}$	Generalized aerodynamic loads of the i^{th} mode
$F_{\mathrm{eq,RNA}}$	Seismic load of the RNA
$F_{hydro,i}$	Generalized hydrodynamic loads of the i^{th} mode
$F_{gra,i}$	Generalized gravity loads of the i^{th} mode
F_s	Soil force
F_{TMD}	TMD force
G_s	Soil shear modulus
H	Length of the support structure
m_i	Modal mass associated with the i^{th} mode

m_{RNA}	Total mass of RNA
m_{T}	TMD mass
m_{WT}	Wind turbine mass
k_{T}	TMD stiffness
k_s	Soil stiffness
q_i	Modal displacement of the i^{th} mode
$\dot{q}_i$	Modal velocity of the i^{th} mode
$\ddot{q}_i$	Modal acceleration of the i^{th} mode
v_s	Structure velocity for soil force calculation
x_{TMD}	TMD displacement
$\dot{x}_{\mathrm{TMD}}$	TMD velocity
$\ddot{x}_{\mathrm{TMD}}$	TMD acceleration
$\ddot{x}_{\mathrm{N}}$	Nacelle acceleration
α_{N}	Nacelle angular velocity
β_s	Hysteresis damping ratio of the soil
λ	Tuned frequency ratio
μ	Tuned mass ratio
ω_m	First-order natural angular frequency of the support structure
ω_{N}	Nacelle translational velocity
ω_i	Angular frequency of the i^{th} mode
ρ_s	Soil density
$\rho(h)$	Mass density of the support structure at the height of h
$\phi_i(h)$	Normalized modal shape of the i^{th} mode of the support structure.
ξ_i	Damping ratio of the i^{th} mode
γ_i	Earthquake participation factor associated with the i^{th} mode

References

[1] Det Norske Veritas - Germanischer Lloyd, Energy transition outlook 2019: A global and regional forecast to 2050. *DNV-GL report*, 2019

[2] Liang, Y., Yu, B., & Wang, L. (2019). Costs and benefits of renewable energy development in China's power industry. *Renewable Energy*, 131, 700-712.

[3] People, planet and prosperity: Raising climate ambition through renewables. https://www.irena.org/publications/2019/Jul/People-Planet-and-Prosperity [accessed 24 April 2020].

[4] International Energy Agency, Offshore wind outlook 2019. World Energy Outlook Special Report. *IEA report*, 2020

[5] Ishihara, T., & Sarwar, M. W. (2008). Numerical and theoretical study on seismic response of wind turbines. *European wind energy conference and exhibition 2008*, Brussels, Belgium.

[6] Butt, U. A. & Ishihara, T. (2012). Seismic load evaluation of wind turbine support structures considering low structural damping and soil structure interaction. *European wind energy association annual event 2012*, Copenhagen, Denmark.

[7] Prowell, I., & Veers, P. (2009). Assessment of wind turbine seismic risk: Existing literature and simple study of tower moment demand. *Sandia National Laboratories Report*, Albuquerque, NM, USA.

[8] Hacıefendioğlu, K. (2012). Stochastic seismic response analysis of offshore wind turbine including fluid- structure- soil interaction. *The Structural Design of Tall and Special Buildings*, 21(12), 867-878.

[9] Haenler, M., Ritschel, U., & Warnke, I. (2006). Systematic modelling of wind turbine dynamics and earthquake loads on wind turbines. *European Wind Energy Conference & Exhibition 2006, Athens*, Greece

[10] Zhao, X., & Maisser, P. (2006). Seismic response analysis of wind turbine towers including soil-structure interaction. *Proceedings of the Institution of Mechanical Engineers, Part K: Journal of Multi-body Dynamics*, 220(1), 53-61.

[11] Ritschel, U., Warnke, I., Kirchner, J., & Meussen, B. (2003). Wind turbines and earthquakes. *World Wind Energy Conference 2003*, Cape Town, South Africa.

[12] Witcher, D. (2005). Seismic analysis of wind turbines in the time domain. *Wind Energy*, 8(1), 81-91.

[13] Santangelo, F., Failla, G., Santini, A. & Arena, F. (2016). Time-domain uncoupled analyses for seismic assessment of land-based wind turbines. *Engineering Structures*, 123, 275-299.

[14] Asareh, M. A. & Prowell, I. (2011). Seismic loading for FAST. *National Renewable Energy Laboratory, Technical Reports No. NREL/SR-5000-53872*, Golden, Colorado, USA.

[15] Asareh, M. A., Prowell, I., Volz, J., & Schonberg, W. (2016). A computational platform for considering the effects of aerodynamic and seismic load combination for utility scale horizontal axis wind turbines. *Earthquake Engineering and Engineering Vibration*, 15(1), 91-102.

[16] Prowell, I., Elgamal, A., Uang, C., & Jonkman, J. (2010). Estimation of seismic load demand for a wind turbine in the time domain. *National Renewable Energy Laboratory (NREL), Technical Report No. NREL/CP-500-47536*, Golden, Colorado, USA.

692 [17] Prowell, I., Elgamal, A. W. M., & Jonkman, J. M. (2010). FAST simulation of wind
693 turbine seismic response. *National Renewable Energy Laboratory, Technical Report No.*
694 *NREL/CP-500-46225*, Golden, Colorado, USA.

695 [18] Asareh, M. A., Schonberg, W. & Volz, J. (2016). Effects of seismic and aerodynamic load
696 interaction on structural dynamic response of multi-megawatt utility scale horizontal axis
697 wind turbines. *Renewable energy*, 86, 49-58.

698 [19] Yang, Y., Ye, K., Li, C., Michailides, C. & Zhang, W. (2018). Dynamic behaviour of wind
699 turbines influenced by aerodynamic damping and earthquake intensity. *Wind Energy*, 21
700 (5), 303-319.

701 [20] Kim, D. H., Lee, S. G. & Lee, I. K. (2014). Seismic fragility analysis of 5 MW offshore
702 wind turbine. *Renewable Energy*, 65, 250-256.

703 [21] Mo, R., Kang, H., Li, M. & Zhao, X. (2017). Seismic fragility analysis of monopile
704 offshore wind turbines under different operational conditions. *Energies*, 10(7), 1037.

705 [22] Alati, N., Failla, G. & Arena, F. (2015). Seismic analysis of offshore wind turbines on
706 bottom-fixed support structures. *Philosophical Transactions of the Royal Society A*, 373
707 (2035), 20140086.

708 [23] Yang, Y., Li, C., Bashir, M., Wang, J., & Yang, C. (2019). Investigation on the sensitivity
709 of flexible foundation models of an offshore wind turbine under earthquake loadings.
710 *Engineering Structures*, 183, 756-769.

711 [24] Yang, Y., Bashir, M., Li, C., & Wang, J. (2019). Analysis of seismic behaviour of an
712 offshore wind turbine with a flexible foundation. *Ocean Engineering*, 178, 215-228.

713 [25] Jonkman, J. M., & Buhl Jr, M. L. (2005). FAST user's guide. *National Renewable Energy*
714 *Laboratory, Technical Report No. NREL/EL-500-38230*, Golden, Colorado, USA.

715 [26] Lackner, M. A., & Rotea, M. A. (2011). Passive structural control of offshore wind
716 turbines. *Wind energy*, 14(3), 373-388.

717 [27] Velarde, J. (2016). Design of monopile foundations to support the DTU 10 MW offshore
718 wind turbine, *Master thesis*, Norwegian University of Science and Technology.

719 [28] Jonkman, J. M. (2003). Modeling of the UAE wind turbine for refinement of FAST_AD.
720 *National Renewable Energy Laboratory, Technical Report No. NREL/TP-500-34755*,
721 Golden, Colorado, USA.

722 [29] C. Bak, R. Bitsche, A. Yde, T. Kim, M. H. Hansen, F. Zahle, et al. Light Rotor: the
723 10-MW reference wind turbine, *Proceedings of the European Wind Energy Association*
724 *(EWEA) Annual Event*, Copenhagen, Demark.

725 [30] Makris, N., & Gazetas, G. (1992). Dynamic pile-soil-pile interaction. Part II: Lateral and
726 seismic response. *Earthquake engineering & structural dynamics*, 21(2), 145-162.

727 [31] Ministry of Housing and Urban-Rural Development of China.(2010). Code for seismic
728 design of buildings. *Chinese Standard, GB 50011-2010*.

729 [32] Al Atik, L. & Abrahamson, N. (2010). An improved method for nonstationary spectral
730 matching. *Earthquake Spectra*, 26(3), 601-617.

731 [33] Jonkman, B. J. (2009). TurbSim user's guide: Version 1.50. *National Renewable Energy*
732 *Laboratory Technical Report No. NREL/TP-500-4619* , Golden, Colorado, USA.

733 [34] Mader, C. L. (2004). *Numerical modeling of water waves*. CRC press, Florida, USA.